Article:
Wang, A., Fei, M., Song, Y. et al. (2024) Scalable Fuzzy Control for Nonlinear DC Microgrids Under Plug-and-Play Operations. IEEE Transactions on Fuzzy Systems, 32 (8). pp. 4747-4758. ISSN: 1063-6706

https://doi.org/10.1109/tfuzz.2024.3412944

Scalable Fuzzy Control for Nonlinear DC Microgrids Under Plug-and-Play Operations

Aimin Wang, *Graduate Student Member, IEEE,* Minrui Fei, Yang Song, *Member, IEEE,* Dajun Du, *Member, IEEE,* Chen Peng, *Senior Member, IEEE,* Kang Li, *Senior Member, IEEE*

***Abstract*—The plugging-in/-out of renewable distributed generation units (DGUs) often alters the microgrid size and coupling terms, resulting in computational burdens and voltage shocks. This paper proposes a novel scalable fuzzy voltage control scheme for nonlinear DC microgrids (DCmGs) composed of DGUs and constant power loads (CPLs) interconnected via power lines. Firstly, a Takagi-Sugeno fuzzy DCmG model with CPL is formulated to capture nonlinear characteristics and diverse transient behaviors. Secondly, a scalable fuzzy control approach is developed to mitigate negative coupling effects of power lines. This is achieved by a novel argument that leverages dissipativity theory to transform such effects into linear matrix inequalities (LMIs) and subsequently imposes constraints on their sequential principal minors. Specifically, the proposed control method operates locally and independently of other DGUs and line couplings, enabling seamless plug-and-play (PnP) operations without updating any controllers. Finally, theoretical results are validated through simulations using the MATLAB/SimPowerSystems toolbox.**

***Index Terms*—DC microgrids (DCmGs), scalable control, plug-and-play (PnP), Takagi-Sugeno fuzzy control, constant power load (CPL).**

I. Introduction

DRIVEN by escalating environmental concerns, the conventional power grid based on synchronous machines has evolved into microgrids [1]–[4], due to the widespread deployment of renewable energy sources (RESs) such as photovoltaic panels and wind turbines [5]–[7]. Microgrids have been regarded as critical components of new power systems, serving as a natural interface to a diverse array of renewable distributed generation units (DGUs) [8]. They can be categorized into alternating-current microgrids (ACmGs) [9] and direct-current microgrids (DCmGs) [10], both capable of operating in islanded or grid-connected modes. Recent advancements in power electronic converters have significantly strengthened the inherent advantages of DCmGs, such as their independence from frequency/reactive power regulation [11]–[13]. Therefore, DCmGs have found increasing applications in various sectors including electric vehicles, marine systems, and spacecraft [14]. However, challenges persist for DCmGs, particularly in maintaining voltage stability with constant power loads (CPLs) and scalability under plug-and-play (PnP) operations of DGUs.

Voltage stability remains a primary concern in DCmGs, particularly under CPLs, due to their nonlinear and negative impedance characteristics, which are known to induce system instabilities [15]. In this regard, Zonetti *et al.* [16] have utilized the Jacobian linearization method to analyze the eigenvalues of linearized DCmGs with CPLs. Various nonlinear control methods (e.g., backstepping method [17]) have been proposed to ensure voltage stability. Alternatively, Liu *et al.* [18] and Gheisarnejad *et al.* [19] have approximated nonlinear DCmGs with CPLs as linear systems, providing robust voltage control methods using polytopic sets and neural network-based approaches, respectively. While effective in ensuring voltage stability, these control methods are constrained by specific DCmG sizes and topologies, thus limiting scalability.

Scalability is also a major concern for DCmGs, especially in scenarios involving PnP operations of renewable DGUs [20]. These operations, causing changes in DCmG size (i.e., the number of DGUs) and power line couplings, present challenges such as computational burdens and transient processes like voltage shocks [7]. A scalable control method, designed locally and independent of the system size and topology, provides a solution to these challenges. It allows seamless integration/removal of DGUs without compromising stability [21]. In this context, it is not surprising that scalable control methods have been extensively investigated in DCmGs. For further details, refer to [7], [9], [20]–[25] and references therein.

Decentralized-based scalable control methods are widely adopted for maintaining DCmG scalability. Specifically, Tucci *et al.* [21], [22] have proposed decentralized scalable voltage control methods for DCmGs by using a separable Lyapunov function (SLF) to mitigate the negative coupling effect of power lines. In this method, the Lyapunov matrix is assumed to have a block-diagonal fixed structure, with all matrix elements other than the diagonal block elements being zero. Furthermore, using the fixed-structure SLF technique to map control design into a linear matrix inequality (LMI) problem, Wang *et al.* [23] and Nahata *et al.* [24] have developed scalable control schemes to guarantee both voltage stability and scalability. However, the use of these scalable control methods may be

This work was supported in part by the Key Project of Science and Technology Commission of Shanghai Municipality under Grant 21190780300; in part by the Natural Science Foundation of China (NSFC) under Grant 62173217, Grant 62203290, and 62303076; in part by the Natural Science Foundation of Shanghai Municipality under Grant 21ZR1423400; in part by the NSFC/Royal Society Cooperation and Exchange Project under Grant 62111530154; and in part by the 111 Project under Grant D18003. *(Corresponding authors: Minrui Fei; Yang Song.)*

A. Wang, M. Fei, Y. Song, D. Du and C. Peng are with the Shanghai Key Laboratory of Power Station Automation Technology, School of Mechatronic Engineering and Automation, Shanghai University, Shanghai 200072, China (e-mail: aiminwang0324@163.com; mrfei@staff.shu.edu.cn; y_song@shu.edu.cn; ddj@i.shu.edu.cn; c.peng@i.shu.edu.cn).

K. Li is with the School of Electronics and Electrical Engineering, University of Leeds, Leeds LS2 9JT, U.K. (e-mail: k.li1@leeds.ac.uk).

TABLE I
COMPARATIVE ANALYSIS BETWEEN THE CONTRIBUTIONS OF THIS PAPER AND THE EXISTING RESULTS IN THE LITERATURE

Ref.[1]	SFC[2]	AC[3]	Sca.[4]	SM[5]	NBPC[6]
[16]	Linear	JLM[7]	✗	–	–
[17]	Nonlinear	BCM[8]	✗	–	–
[18]	ANSL[9]	PS[10]	✗	–	–
[19]	ANSL	NN[11]	✗	–	–
[31]	ANSL	FR[12]	✗	–	–
[21]	Linear	–	✓	SLF[13]	✗
[22]	Linear	–	✓	SLF	✗
[23]	Linear	–	✓	SLF	✗
[24]	Linear	–	✓	SLF	✗
[9]	Linear (AC)	–	✓	SLF	✗
[25]	Linear (AC)	–	✓	SLF	✗
†[14]	ANSL	FR	✓	ASLF[15]	✓

[1]References. [2]System form with CPLs.
[3]Address CPLs. [4]Scalability. [5]Structured matrix.
[6]No bumpless scheme/pre-filter/compensator.
[7]Jacobian linearization method. [8]Backstepping method.
[9]Approximating the nonlinear system as a linear.
[10]Polytopic set. [11]Neural network. [12]Fuzzy rule.
[13]Separable Lyapunov function. [14]This paper.
[15]Avoid separable Lyapunov function.

limited, as structured Lyapunov matrices often render LMI-based controller designs numerically infeasible or conservative [25].

Motivated by the above observations, the following challenges will be addressed:

1) How to better model the nonlinear DCmG systems with CPLs?
2) How to design a new scalable control to overcome the limitations arising from SLF?
3) How to enable seamless PnP requirements of renewable DGUs?

To deal with these challenges, this paper proposes a novel scalable fuzzy control scheme for nonlinear DCmGs under PnP operations of DGUs with CPLs. Table I presents a comparative analysis with existing methods. It can be clearly found that existing results have mainly focused on voltage control without scalable property or scalability using the SLF technique. In contrast, the proposed method ensures voltage stability and scalability while eliminating the assumptions on the block-diagonal fixed structure of the Lyapunov matrix. The main contributions of this paper are summarized as follows:

1) Unlike linear [16], nonlinear [17], and approximated linear modeling methods [18], [19] in which the nonlinear characteristic of CPLs is considered in DCmGs, this paper exactly represents the nonlinear DCmG system in a Takagi-Sugeno (T-S) fuzzy model due to its efficiency in characterizing the nonlinear nature and different transient performance of CPLs.
2) Compared to existing scalable control methods based on the SLF technique [21]–[23], this paper proposes a novel scalable fuzzy control scheme for DCmGs with CPLs, without structured and diagonal assumptions for Lyapunov matrices. Moreover, unlike previous methods that may result in LMI-based controller designs numerically infeasible or conservative, the proposed control method enhances solvability and reduces the conservativeness by eliminating the strict constraints on Lyapunov matrix.
3) The negative effects of line couplings can be removed by transforming them into LMI conditions and subsequently imposing constraints on their sequential principal minors. Therefore, the proposed scalable fuzzy control is carried out locally at the subsystem level, without requiring the knowledge of line couplings and neighboring DGUs. Specifically, it allows the seamless plugging-in/-out of DGUs in a PnP fashion, without the need to update controllers of neighboring DGUs.

This paper is structured as follows: Section II introduces both local and global DCmG models with CPLs. Section III formulates problems encountered under PnP operations. Scalable stability analysis and controller design are detailed in Section IV. Section V presents simulation results. Finally, this work is concluded in Section VI.

Notations: The set of all $m \times n$ real matrices is denoted by $\mathbb{R}^{m\times n}$. Null and identity matrices with appropriate dimensions are represented as $\mathbf{0}$ and $\mathbf{I}$. The notation $Z < 0$ (or $Z > 0$) signifies that the matrix $Z \in \mathbb{R}^{n\times n}$ is negative definite (or positive definite). The symbol $*$ represents the symmetric term in a symmetric matrix. Given $z \in \mathbb{R}^n$, $\mathrm{diag}\{z\} \in \mathbb{R}^{n\times n}$ corresponds to the associated diagonal matrix with elements of z on the diagonal. $X(i,j)$ denotes the element in position (i,j) of matrix $X = [X(i,j)]_{i\in m, j\in n}$. The notation $\mathbb{S}_i$ represents a local subsystem of the global system $\mathbf{S}_n$ that is composed of n subsystems. Additionally, $\mathbf{S}_n|\mathbb{S}^+_{n+1}$ denotes that a new subsystem $\mathbb{S}_{n+1}$ is plugged in $\mathbf{S}_n$, while $\mathbf{S}_n|\mathbb{S}^-_{n-1}$ represents that an existing subsystem $\mathbb{S}_{n-1}$ is unplugged from $\mathbf{S}_n$.

II. MODEL OF DCMGS WITH CPLS

In this section, the DGU model with CPL is presented first. Next, the state-space model of a local subsystem is formulated. Then, the structure of the fuzzy controller is provided. Finally, the closed-loop global DCmG consisting of n DGUs is given.

Note that the information flow within DCmGs is represented as a connected graph $\mathcal{G} = (\mathcal{V}, \mathcal{E})$ comprising a node set $\mathcal{V} = \{1, 2, ..., n\}$ and an edge set $\mathcal{E} \subset \mathcal{V} \times \mathcal{V}$. The set of neighbors of node i, $i \in \mathcal{V}$, is denoted as $\mathcal{N}_i$. As shown in Fig. 1, each subsystem (node) is composed of a renewable DGU, a local controller, and a CPL. These nodes establish decentralized interconnections solely via power lines (edges), serving as the exclusive communication medium and presented by an RL circuit [26]. Notably, the voltage references in each DGU are set to be slight differences to ensure current flow through power lines in the asymptotic regime [27].

A. Electrical Model of A DGU With CPL

Fig. 1 illustrates the structure of DCmG systems, where each DGU comprises a DC voltage source, a buck converter, and a series RLC filter. The buck converter serves as the interface

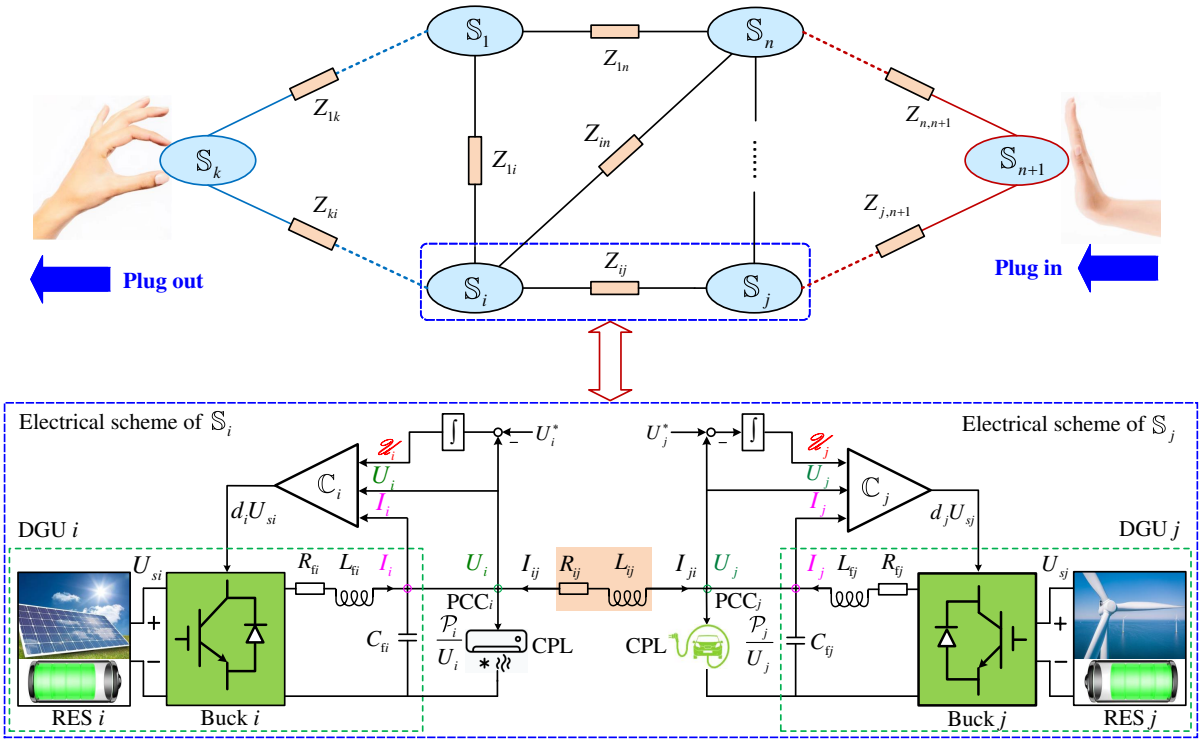

Fig. 1. Framework of scalable fuzzy control for nonlinear DCMGs interconnected via power lines Z_{ij}

between the controller and DGU, regulating the power supply to CPL. Notably, the local CPL is modeled as a current sink, with its current injection determined by its power divided by the CPL voltage [15]. For simplicity, it is assumed that the local CPL is connected to the DGU terminal. Indeed, even if load buses are located elsewhere, they can be mapped to the point of common coupling (PCC) using Kron reduction [28].

Using the quasi-stationary-line (QSL) approximation for power lines [29], one has

$$I_{ij} = \sum_{j\in\mathcal{N}_i} \frac{1}{R_{ij}} \left(U_j - U_i\right). \tag{1}$$

By applying Kirchhoff voltage and current laws to the DCmG framework illustrated in Fig. 1, one obtains

$$\begin{cases} \dot{U}_i = \dfrac{1}{C_{\mathrm{f}i}} I_i + \displaystyle\sum_{j\in\mathcal{N}_i} \frac{1}{C_{\mathrm{f}i} R_{ij}} \left(U_j - U_i\right) - \frac{1}{C_{\mathrm{f}i}} \frac{\mathcal{P}_i}{U_i} \\ \dot{I}_i = -\dfrac{R_{\mathrm{f}i}}{L_{\mathrm{f}i}} I_i - \dfrac{1}{L_{\mathrm{f}i}} U_i + \dfrac{d_i}{L_{\mathrm{f}i}} U_{si} \\ \dot{\mathscr{U}}_i = U_i^* - U_i \end{cases} \tag{2}$$

where U_i and U_j denote the voltage signals at PCC i and j, respectively. I_i represents the filter current. $R_{\mathrm{f}i}$, $L_{\mathrm{f}i}$, $C_{\mathrm{f}i}$, and R_{ij} are the electrical parameters of the RLC filter and power line. $\mathcal{P}_i$ denotes the constant power demand of CPL. $d_i \in [0,1]$ is the duty cycle of the buck converter, and U_{si} represents the voltage of its power source. Note that U_{si} is large enough to avoid saturation of d_i [27]. Moreover, U_i^* represents a predefined reference voltage, and $\mathscr{U}_i$ denotes the integrator state.

Remark 1*:* Note that the electrical model (2) is based on the following considerations:

1) The representation of RES through an ideal DC voltage source, which is a pragmatic approach considering the typical slow timescale oscillations in RES-generated power. Additionally, RES installations often incorporate energy storage units to effectively dampen stochastic oscillations [21].
2) The utilization of the QSL approximation to achieve neutral interactions among renewable DGUs. This approximation assumes predominantly resistive characteristics in power lines and its validity is supported by singular perturbation theory [29].
3) The use of an integration process to rectify static errors in voltage tracking, ensuring precise alignment of the controlled voltage U_i with the prescribed reference voltage U_i^* [30].

For an equilibrium point $[U_{0i}, U_{0j}, I_{0i}, \mathscr{U}_{0i}, d_{0i}, U_{0i}^*]$, the constant power demand $\mathcal{P}_i$ of CPL must satisfy [31]

$$\mathcal{P}_i < \min\left\{ \frac{U_{si}}{4R_{\mathrm{f}i}}, \frac{R_{\mathrm{f}i} C_{\mathrm{f}i} U_{0i}^2}{L_{\mathrm{f}i}} \right\} = \mathcal{P}_i^{\max} \tag{3}$$

where $\mathcal{P}_i^{\max}$ denotes the maximum power demand of CPL by linearizing the dynamics (2) around the equilibrium point. This condition guarantees that the Hurwitz property of the Jacobian matrix of (2) with a negative real part, ensuring the existence of a real operating point.

Due to the nonlinear nature of CPL (i.e., $\frac{\mathcal{P}_i}{U_i(t)}$), stable operation of (2) is not ensured. To apply Lyapunov stability theory effectively, the dynamical system must possess an equilibrium point located at the origin. This prerequisite can be fulfilled by implementing a change of coordinates [32].

Subsequently, with the transformation indicated by

$$\overline{U}_i = U_i - U_{0i}, \overline{U}_j = U_j - U_{0j}, \overline{I}_i = I_i - I_{0i},$$
$$\overline{\mathscr{U}}_i = \mathscr{U}_i - \mathscr{U}_{0i}, \overline{d}_i = d_i - d_{0i}, \overline{U}_i^* = U_i^* - U_{0i}^*,$$

the dynamics (2) can be rewritten as

$$\begin{cases} \dot{\overline{U}}_i = \dfrac{1}{C_{\mathrm{fi}}}\overline{I}_i + \displaystyle\sum_{j\in\mathscr{N}_i} \frac{1}{C_{\mathrm{fi}}R_{ij}}\left(\overline{U}_j - \overline{U}_i\right) - \frac{\mathcal{P}_i}{C_{\mathrm{fi}}} f_i(\overline{U}_i) \\ \dot{\overline{I}}_i = -\dfrac{R_{\mathrm{fi}}}{L_{\mathrm{fi}}}\overline{I}_i - \dfrac{1}{L_{\mathrm{fi}}}\overline{U}_i + \dfrac{\overline{d}_i}{L_{\mathrm{fi}}}U_{\mathrm{si}} \\ \dot{\overline{\mathscr{U}}}_i = \overline{U}_i^* - \overline{U}_i \end{cases} \tag{4}$$

where $f_i(\overline{U}_i)$ is a nonlinear term caused by CPL, that is

$$f_i(\overline{U}_i) = \frac{\overline{U}_i}{U_{0i}(\overline{U}_i + U_{0i})}. \tag{5}$$

Remark 2: To cope with the nonlinearity term $f_i(\overline{U}_i)$, the Jacobian linearization method was introduced in [16]. However, the approach failed to simultaneously improve settling time and overshooting performance [33]. The nonlinear backstepping control method [17] was proposed to ensure voltage stability; however, it may not completely address the nonlinearities of CPLs in the presence of noise [34]. Moreover, works [18] and [19] approximated the nonlinear DCmG system with linear systems. However, such linear controllers may reduce the closed-loop system performance. Specifically, their applicability is non-scalable with various DCmG sizes and topologies.

B. State-Space Model of T-S Fuzzy DCmG

In this paper, we adopt a T-S fuzzy modeling approach based on the sector nonlinearity method [35], [36] to precisely represent the nonlinear DCmG model with CPL. This modeling technique adeptly captures the behavior of nonlinear systems with smooth behavior. Notably, T-S fuzzy models feature a linear consequent part, facilitating the application of established theories in linear control to nonlinear systems without cumbersome linearization procedures [37]–[40]. By employing the T-S fuzzy framework, we avoid the necessity for linearization, ensuring accurate representation of the nonlinear nature and different transient performance of CPL.

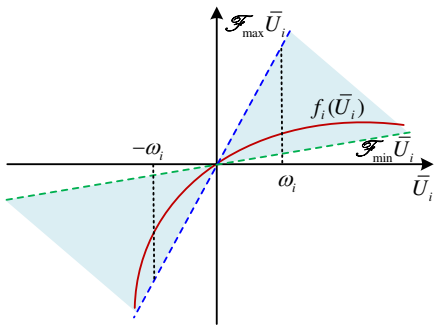

Fig. 2. Sector nonlinearity approach for CPL [36]. Red solid line: nonlinearity of CPL. Blue dashed line: upper bound of the sector. Green dashed line: lower bound of the sector.

The nonlinear term $f_i(\overline{U}_i)$ and its corresponding sectors is plotted in Fig. 2. It is shown that $f_i(\overline{U}_i)$ falls inside two linear sectors, for a given region $-\omega_i \le \overline{U}_i \le \omega_i$ with positive scalar ω_i, that is

$$\mathscr{F}_{\min}\overline{U}_i \le f_i(\overline{U}_i) \le \mathscr{F}_{\max}\overline{U}_i \tag{6}$$

where $\mathscr{F}_{\min}$ and $\mathscr{F}_{\max}$ denote the lower and upper slopes, with the following formats:

$$\mathscr{F}_{\min} = \frac{1}{U_{0i}(U_{0i}+\omega_i)}, \ \mathscr{F}_{\max} = \frac{1}{U_{0i}(U_{0i}-\omega_i)}. \tag{7}$$

Thus, the nonlinear term $f_i(\overline{U}_i)$ can be decomposed to

$$\begin{cases} f_i(\overline{U}_i) = M_1\mathscr{F}_{\min}\overline{U}_i + M_2\mathscr{F}_{\max}\overline{U}_i \\ M_1 + M_2 = 1 \end{cases} \tag{8}$$

where $0 \le M_h \le 1$ for $h = 1, 2$ denotes the normalized membership functions as

$$M_1 = \frac{\mathscr{F}_{\max}\overline{U}_i - f_i(\overline{U}_i)}{(\mathscr{F}_{\max} - \mathscr{F}_{\min})\overline{U}_i}, M_2 = \frac{f_i(\overline{U}_i) - \mathscr{F}_{\min}\overline{U}_i}{(\mathscr{F}_{\max} - \mathscr{F}_{\min})\overline{U}_i}. \tag{9}$$

Therefore, the membership functions of the T-S fuzzy model are obtained systematically. The fuzzy IF-THEN rules for DCmG with CPL are obtained as

Rule 1: IF $\frac{f_i(\overline{U}_i)}{\overline{U}_i}$ is $\mathscr{F}_{\min}$ THEN $\dot{x}_i(t) = A_{ii,1}x_i(t) + B_iu_i(t) + D_iv_i(t) + \sum_{j\in\mathscr{N}_i} A_{ij}x_j(t)$.

Rule 2: IF $\frac{f_i(\overline{U}_i)}{\overline{U}_i}$ is $\mathscr{F}_{\max}$ THEN $\dot{x}_i(t) = A_{ii,2}x_i(t) + B_iu_i(t) + D_iv_i(t) + \sum_{j\in\mathscr{N}_i} A_{ij}x_j(t)$.

Then, by utilizing the singleton fuzzifier, product inference engine, and center of average defuzzifier [38], the equivalent T-S fuzzy DCmG system can be described by the following state-space model:

$$\mathbb{S}_i : \begin{cases} \dot{x}_i(t) = \displaystyle\sum_{h=1}^{2} M_h\Big(A_{ii,h}x_i(t) + B_iu_i(t) + D_iv_i(t) \\ \qquad\qquad + \displaystyle\sum_{j\in\mathscr{N}_i} A_{ij}x_j(t)\Big) \\ y_i(t) = C_ix_i(t) \end{cases} \tag{10}$$

where $x_i = [\overline{U}_i, \overline{I}_i, \overline{\mathscr{U}}_i]^T$ denotes the state vector of subsystem $\mathbb{S}_i$ and x_j represents the state vector of $\mathbb{S}_j$, for $i \in \mathcal{V}$, $j \in \mathscr{N}_i$. $v_i = \overline{U}_i^*$ denotes the external disturbance. Moreover, $y_i(t)$ represents the measurable output and we assume $y_i(t) = x_i(t)$, i.e., $C_i = \mathbf{I}$. $u_i = \overline{d}_iU_{\mathrm{si}}$ denotes the control action to the buck converter. Matrix A_{ij} represents the line coupling between $\mathbb{S}_i$ and $\mathbb{S}_j$, and is referred to as the coupling matrix. Related system matrices are given as

$$A_{ii,1} = \left[\begin{array}{c|c|c} -\displaystyle\sum_{j\in\mathscr{N}_i}\frac{1}{C_{\mathrm{fi}}R_{ij}} - \frac{\mathcal{P}_i}{C_{\mathrm{fi}}}\mathscr{F}_{\min} & \frac{1}{C_{\mathrm{fi}}} & 0 \\ \hline -\frac{1}{L_{\mathrm{fi}}} & -\frac{R_{\mathrm{fi}}}{L_{\mathrm{fi}}} & 0 \\ \hline -1 & 0 & 0 \end{array}\right],$$

$$A_{ii,2} = \left[\begin{array}{c|c|c} -\displaystyle\sum_{j\in\mathscr{N}_i}\frac{1}{C_{\mathrm{fi}}R_{ij}} - \frac{\mathcal{P}_i}{C_{\mathrm{fi}}}\mathscr{F}_{\max} & \frac{1}{C_{\mathrm{fi}}} & 0 \\ \hline -\frac{1}{L_{\mathrm{fi}}} & -\frac{R_{\mathrm{fi}}}{L_{\mathrm{fi}}} & 0 \\ \hline -1 & 0 & 0 \end{array}\right],$$

$$A_{ij}=\left[\begin{array}{c|c|c} \frac{1}{C_{\mathrm{f}i}R_{ij}} & 0 & 0 \\ \hline 0 & 0 & 0 \\ \hline 0 & 0 & 0 \end{array}\right], B_i=\left[\begin{array}{c} 0 \\ \frac{1}{L_{\mathrm{f}i}} \\ 0 \end{array}\right], D_i=\left[\begin{array}{c} 0 \\ 0 \\ 1 \end{array}\right].$$

C. Decentralized Structure of Fuzzy Controller

We will design a fuzzy aggregation of several linear controllers for $\mathbb{S}_i$. Before that, we ensure the controllability of the pair $(A_{ii,h}, B_i)$ through the following proposition.

Proposition 1*:* The pair $(A_{ii,h}, B_i)$ is controllable.

Proof: Using the definition of controllability matrix [41], one obtains

$$\begin{aligned}\mathcal{M}_i &= \left[\begin{array}{ccc} B_i & A_{ii,h}B_i & A_{ii,h}^2B_i \end{array}\right] \\ &= \left[\begin{array}{ccc} 0 & \frac{1}{L_{\mathrm{f}i}C_{\mathrm{f}i}} & \frac{L_{\mathrm{f}i}A_{ii,h}(1,1)-R_{\mathrm{f}i}}{L_{\mathrm{f}i}^2C_{\mathrm{f}i}} \\ \frac{1}{L_{\mathrm{f}i}} & -\frac{R_{\mathrm{f}i}}{L_{\mathrm{f}i}^2} & \frac{C_{\mathrm{f}i}R_{\mathrm{f}i}^2-L_{\mathrm{f}i}}{L_{\mathrm{f}i}^3C_{\mathrm{f}i}} \\ 0 & 0 & -\frac{1}{L_{\mathrm{f}i}C_{\mathrm{f}i}} \end{array}\right]\end{aligned}$$

where $A_{ii,h}(1,1)$ is the element in position (1,1) of the matrix $A_{ii,h}$. As all electrical parameters in DCmGs are positive, the matrix $\mathcal{M}_i$ always has full rank, i.e., rank($\mathcal{M}_i$) = 3. Thus, the proof is completed.

Based on Proposition 1, a local state-feedback fuzzy controller $\mathbb{C}_i$ will be implemented in each subsystem $\mathbb{S}_i$. For $h = 1, 2$ and $i \in \mathcal{V}$, the fuzzy controller is designed as

$$\mathbb{C}_i : u_i(t) = \sum_{h=1}^{2} M_h K_{i,h} x_i(t) \tag{11}$$

where $K_{i,h} \in \mathbb{R}^{1\times 3}$ represents the multivariable PI controller gain for different membership functions.

Remark 3*:* Note that the control architecture in this paper is decentralized and the computation of $u_i(t)$ only requires the state of each subsystem. The choice is guided by the specific characteristics of the investigated system: DCmG system interconnected solely via physical power lines without the involvement of any communication network. This decision is underpinned by three key advantages over a distributed architecture [26]:

1) Scalability: Decentralized architecture demonstrates superior scalability as the addition/removal of subsystems minimally impacts overall system complexity. Moreover, plugging-in/-out operations do not necessitate modifications to the control structure.
2) Robustness: Decentralized control systems operate independently, rendering them more resilient to communication failures, attacks, or delays. This robustness is crucial in systems lacking reliable communication network channels, such as power line-interconnected DCmGs.
3) Simplicity: Decentralized architecture offers simplicity in implementation and analysis compared to distributed approaches. By avoiding complex communication protocols, it simplifies control strategy development and deployment, particularly in real-world scenarios with limited computational resources.

D. The Closed-Loop Global DCmGs With n DGUs

The individual local subsystem, denoted as $\mathbb{S}_i$, can be expanded into a global DCmGs, represented as $\mathbf{S}_n$, interconnected in a decentralized style through power lines [26]. Thus, the overall model of the collective global DCmGs is formulated as follows:

$$\mathbf{S}_n : \begin{cases} \dot{\boldsymbol{x}}(t) = \sum_{h=1}^{2} M_h\Big((\boldsymbol{A}_h + \boldsymbol{B}\boldsymbol{K}_h)\boldsymbol{x}(t) + \boldsymbol{D}\boldsymbol{v}(t)\Big) \\ \boldsymbol{y}(t) = \boldsymbol{C}\boldsymbol{x}(t) \end{cases} \tag{12}$$

where

$$\begin{aligned} \boldsymbol{x}(t) &= \left[x_1^T(t), x_2^T(t), \ldots, x_n^T(t)\right]^T \\ \boldsymbol{v}(t) &= \left[v_1^T(t), v_2^T(t), \ldots, v_n^T(t)\right]^T \\ \boldsymbol{y}(t) &= \left[y_1^T(t), y_2^T(t), \ldots, y_n^T(t)\right]^T \end{aligned}$$

and

$$\begin{aligned} \boldsymbol{A}_h &= \left[\begin{array}{cccc} A_{11,h} & A_{12} & \cdots & A_{1n} \\ A_{21} & A_{22,h} & \cdots & A_{2n} \\ \vdots & \vdots & \ddots & \vdots \\ A_{n1} & A_{n2} & \cdots & A_{nn,h} \end{array}\right] \\ \boldsymbol{B} &= \mathrm{diag}\left\{B_1, B_2, \ldots, B_n\right\} \\ \boldsymbol{C} &= \mathrm{diag}\left\{C_1, C_2, \ldots, C_n\right\} \\ \boldsymbol{D} &= \mathrm{diag}\left\{D_1, D_2, \ldots, D_n\right\} \\ \boldsymbol{K}_h &= \mathrm{diag}\left\{K_{1,h}, K_{2,h}, \ldots, K_{n,h}\right\}. \end{aligned}$$

III. Problem Formulation

In this section, we establish the problem formulation for scalable stability analysis and controller design for nonlinear DCmGs under PnP operations.

Dissipativity theory: The concept of dissipativity theory establishes a relationship between the internally stored energy of a system and a generalized energy supply function $\mathscr{F}_i(y_i(t), v_i(t))$. The stored energy is quantified using an energy storage function $V_i(x_i(t))$, akin to the Lyapunov function.

Definition 1*:* [42] The system $\mathbb{S}_i$ is dissipativity with respect to the energy supply rate $\mathscr{F}(y_i(t), v_i(t))$ if there exists a non-negative storage function $V_i(x_i(t))$ such that, for all $t > t_0 \geq 0$, the following condition holds:

$$V(x_i(t)) - V(x_i(t_0)) \leq \int_{t_0}^{t} \mathscr{F}(y_i(\tau), v_i(\tau))d\tau$$

where $x_i(t)$ represents the state at time t arising from the initial condition $x_i(t_0)$. Furthermore, $\mathcal{QSR}$-dissipativity is guaranteed if the system $\mathbb{S}_i$ is dissipativity with respect to

$$\begin{aligned}\mathscr{F}(y_i(\tau), v_i(\tau)) = y_i^T(\tau)\mathcal{Q}_i y_i(\tau) + 2y_i^T(\tau)\mathcal{S}_i v_i(\tau) \\ + v_i^T(\tau)\mathcal{R}_i v_i(\tau)\end{aligned}$$

where $\mathcal{Q}_i = \mathcal{Q}_i^T$, $\mathcal{R}_i = \mathcal{R}_i^T$.

Then, we will analyze the $\mathcal{QSR}$-dissipativity of global DCmGs $\mathbf{S}_n$ as follows.

Proposition 2*:* The dissipativity of closed-loop global DCmGs $\mathbf{S}_n$ interconnected with power lines is guaranteed, if there exist matrices $\boldsymbol{K}_h, \boldsymbol{\mathcal{S}}$, symmetric matrices $\boldsymbol{\mathcal{Q}}, \boldsymbol{\mathcal{R}}$, and

a positive definite Lyapunov matrix $\boldsymbol{P}$ with

$$\begin{aligned}\boldsymbol{\mathcal{Q}} &= \text{diag}\left\{\mathcal{Q}_1, \mathcal{Q}_2, \ldots, \mathcal{Q}_n\right\},\\ \boldsymbol{\mathcal{S}} &= \text{diag}\left\{\mathcal{S}_1, \mathcal{S}_2, \ldots, \mathcal{S}_n\right\},\\ \boldsymbol{\mathcal{R}} &= \text{diag}\left\{\mathcal{R}_1, \mathcal{R}_2, \ldots, \mathcal{R}_n\right\},\\ \boldsymbol{P} &= \text{diag}\{P_1, P_2, \ldots, P_n\},\end{aligned}$$

such that the following condition holds:

$$\boldsymbol{\Phi}_h = \left[\begin{array}{c|c} \boldsymbol{P}\boldsymbol{A}_h + \boldsymbol{A}_h^T\boldsymbol{P} - \boldsymbol{\mathcal{Q}} + \boldsymbol{\Phi}_{11} & \boldsymbol{P}\boldsymbol{D} - \boldsymbol{\mathcal{S}} \\ \hline * & -\boldsymbol{\mathcal{R}} \end{array}\right] < 0 \quad (13)$$

where $\boldsymbol{\Phi}_{11} = \boldsymbol{P}\boldsymbol{B}\boldsymbol{K}_h + \boldsymbol{K}_h^T\boldsymbol{B}^T\boldsymbol{P}$.

Proof: By choosing a storage function as

$$\boldsymbol{V}(\boldsymbol{x}(t)) = \sum_{i=1}^{n} V_i(x_i(t)) = \boldsymbol{x}^T(t)\boldsymbol{P}\boldsymbol{x}(t) \quad (14)$$

where the storage function $\boldsymbol{V}(\boldsymbol{x}(t))$ collects all local storage function $V_i(x_i(t))$.

Next, by taking the time derivative along the solution of $\mathbf{S}_n$, one obtains

$$\dot{\boldsymbol{V}}(\boldsymbol{x}(t)) = 2\boldsymbol{x}^T(t)\boldsymbol{P}\dot{\boldsymbol{x}}(t). \quad (15)$$

For any non-zero bounded $\boldsymbol{v}(t)$, we define the following performance requirement:

$$J(\tau) = \int_0^\tau \left[\begin{array}{c} \boldsymbol{y}(t) \\ \boldsymbol{v}(t) \end{array}\right]^T \left[\begin{array}{cc} \boldsymbol{\mathcal{Q}} & \boldsymbol{\mathcal{S}} \\ \boldsymbol{\mathcal{S}}^T & \boldsymbol{\mathcal{R}} \end{array}\right]^T \left[\begin{array}{c} \boldsymbol{y}(t) \\ \boldsymbol{v}(t) \end{array}\right] dt. \quad (16)$$

Then, under the zero initial condition, i.e., $\boldsymbol{x}_0 = 0$, we can obtain following expression by combining (15) and (16):

$$\begin{aligned} J^\star =& \boldsymbol{V}(\boldsymbol{x}(\tau)) - J(\tau)\\ =& \int_0^\tau \Big\{\dot{\boldsymbol{V}}(\boldsymbol{x}(t)) - \boldsymbol{y}^T(t)\boldsymbol{\mathcal{Q}}\boldsymbol{y}(t)\\ & - 2\boldsymbol{y}^T(t)\boldsymbol{\mathcal{S}}\boldsymbol{v}(t) - \boldsymbol{v}^T(t)\boldsymbol{\mathcal{R}}\boldsymbol{v}(t)\Big\}dt\\ =& \int_0^\tau \left\{\boldsymbol{\zeta}^T(t)\sum_{h=1}^{2} M_h\boldsymbol{\Phi}_h\boldsymbol{\zeta}(t)\right\} dt \end{aligned} \quad (17)$$

where $\boldsymbol{\zeta}(t) = \left[\boldsymbol{x}^T(t), \boldsymbol{v}^T(t)\right]^T$ and $\boldsymbol{y}^T(t) = \boldsymbol{C}\boldsymbol{x}(t)$ with $\boldsymbol{C} = \mathbf{I}$.

According to $\boldsymbol{\Phi}_h < 0$ in (13), one has $J^\star < 0$, which ensures the $\mathcal{QSR}$-dissipativity of global DCmGs given in Definition 1. Thus, the proof is completed.

Remark 4*:* The dissipativity condition presented in Proposition 2 relies on global information encompassing all local subsystems and power line couplings. Specifically, the system state matrix $\boldsymbol{A}_h$ in (12) collects the dynamics of all subsystems and power lines, comprising elements $A_{ii,h}$ and A_{ij}, for $h = 1, 2, i \in \mathcal{V}, j \in \mathcal{N}_i$. We define $\boldsymbol{A}_{\mathrm{D},h} = \text{diag}\{A_{11,h}, A_{22,h}, \ldots, A_{nn,h}\}$ to exclusively capture the state transition matrices of individual subsystems. Thus, $\boldsymbol{A}_{\mathrm{C}} = \boldsymbol{A}_h - \boldsymbol{A}_{\mathrm{D},h}$ denotes the coupling matrix, as utilized in [9], [21]–[23]. Based on this, the dissipativity stability condition (13) can be decomposed into two components as follows:

$$\boldsymbol{\Phi}_h = \boldsymbol{\Phi}_{\mathrm{D},h} + \boldsymbol{\Phi}_{\mathrm{C}} \quad (18)$$

where $\boldsymbol{\Phi}_{\mathrm{D},h}$ exclusively accounts for the dissipativity condition of individual subsystems, i.e.,

$$\boldsymbol{\Phi}_{\mathrm{D},h} = \left[\begin{array}{c|c} \boldsymbol{P}\boldsymbol{A}_{\mathrm{D},h} + \boldsymbol{A}_{\mathrm{D},h}^T\boldsymbol{P} - \boldsymbol{\mathcal{Q}} + \boldsymbol{\Phi}_{11} & \boldsymbol{P}\boldsymbol{D} - \boldsymbol{\mathcal{S}} \\ \hline * & -\boldsymbol{\mathcal{R}} \end{array}\right] \quad (19)$$

and $\boldsymbol{\Phi}_{\mathrm{C}}$ represents the coupling effects of power lines, i.e.,

$$\boldsymbol{\Phi}_{\mathrm{C}} = \left[\begin{array}{c|c} \boldsymbol{P}\boldsymbol{A}_{\mathrm{C}} + \boldsymbol{A}_{\mathrm{C}}^T\boldsymbol{P} & \mathbf{0} \\ \hline \mathbf{0} & \mathbf{0} \end{array}\right]. \quad (20)$$

As discussed in Remark 4, the integration/disconnection of renewable DGUs often induces switching behavior and dynamic fluctuations due to changes in the coupling matrix $\boldsymbol{A}_{\mathrm{C}}$ within $\boldsymbol{\Phi}_{\mathrm{C}}$. These variations frequently result in voltage transients and increase computational complexity [7], [23]. Therefore, there is a critical need to develop a scalable approach for stability analysis and controller design capable of facilitating seamless PnP operations. Such an approach should rely solely on the knowledge of subsystem dynamics, while disregarding the effects of dynamic coupling. In this context, the problems of this paper are formulated as follows:

1) *Scalable dissipativity analysis:* Present a dissipativity condition executed at the subsystem level, ensuring the stability of global DCmG systems by checking local conditions.
2) *Scalable controller design:* Develop a new control algorithm that relies solely on local information independent of power line couplings, thereby making it adaptable to changes in DCmG size and topology.
3) *Seamless PnP operations:* Ensure that the plugging in/out of a DGU with CPL does not necessitate any adjustments to the existing control structures of all DGUs, while maintaining the dissipativity of both local and global DCmG systems.

IV. SCALABLE DISSIPATIVITY ANALYSIS AND CONTROLLER DESIGN

In this section, we present the scalable dissipativity analysis and controller design that can be carried out locally, while removing the coupling effect on dissipativity conditions.

A. Scalable Dissipativity Analysis at a Subsystem Level

It is evident that the coupling matrix $\boldsymbol{\Phi}_{\mathrm{C}}$ (20) exhibits solely a non-zero element at position (1,1); therefore, our analysis is focused exclusively on each block of $\boldsymbol{P}\boldsymbol{A}_{\mathrm{C}} + \boldsymbol{A}_{\mathrm{C}}^T\boldsymbol{P}$ characterized by the following structure:

$$P_iA_{ij} + A_{ij}^TP_i = \left[\begin{array}{c|c|c} \frac{2P_i(1,1)}{C_{\mathrm{f}i}R_{ij}} & \frac{P_i(1,2)}{C_{\mathrm{f}i}R_{ij}} & \frac{P_i(1,3)}{C_{\mathrm{f}i}R_{ij}} \\ \hline \frac{P_i(1,2)}{C_{\mathrm{f}i}R_{ij}} & 0 & 0 \\ \hline \frac{P_i(1,3)}{C_{\mathrm{f}i}R_{ij}} & 0 & 0 \end{array}\right]. \quad (21)$$

To mitigate the coupling effect, previous works [9], [21]–[24] used the SLF method. This method assumes a block-diagonal fixed structure for the Lyapunov matrix, where all matrix elements other than the diagonal block elements are zero, that is $P_i(1,2) = 0$ and $P_i(1,3) = 0$. However, this approach often leads to numerically infeasible or conservative LMI-based controller designs [25].

To cope with this challenge, we introduce energy supply rates as additional design variables and assume the existence of a non-zero scalar δ (a parameter common to all DGUs). This leads to

$$\mathbf{\Phi}_h = \mathbf{\Phi}'_{\mathrm{D},h} + \mathbf{\Phi}'_{\mathrm{C}} \tag{22}$$

where

$$\mathbf{\Phi}'_{\mathrm{D},h} = \begin{bmatrix} \boldsymbol{P}\boldsymbol{A}_{\mathrm{D},h} + \boldsymbol{A}_{\mathrm{D},h}^T\boldsymbol{P} - (1+\delta)\boldsymbol{\mathcal{Q}} + \mathbf{\Phi}^{11} & \boldsymbol{P}\boldsymbol{D} - \boldsymbol{\mathcal{S}} \\ * & -\boldsymbol{\mathcal{R}} \end{bmatrix} \tag{23a}$$

$$\mathbf{\Phi}'_{\mathrm{C}} = \begin{bmatrix} \boldsymbol{P}\boldsymbol{A}_{\mathrm{C}} + \boldsymbol{A}_{\mathrm{C}}^T\boldsymbol{P} + \delta\boldsymbol{\mathcal{Q}} & \mathbf{0} \\ \mathbf{0} & \mathbf{0} \end{bmatrix}. \tag{23b}$$

Based on this, a scalable dissipativity analysis of global DCmGs $\mathbf{S}_n$ is summarized as follows.

Theorem 1*:* The dissipativity and scalability of closed-loop global DCmGs $\mathbf{S}_n$ interconnected with power lines are guaranteed, if there exists positive definite matrix $P_i = [P_i(p,q)]_{p\in 3,q\in 3}$, symmetric matrices $\mathcal{Q}_i = [\mathcal{Q}_i(p,q)]_{p\in 3,q\in 3}, \mathcal{R}_i$, and suitable matrices $\mathcal{S}_i, K_{i,h}$ for $h = 1,2$ such that the following conditions hold:

$$\Upsilon_{11} < 0 \tag{24}$$

$$\begin{vmatrix} \Upsilon_{11} & \Upsilon_{12} \\ \Upsilon_{12} & \delta Q_i(2,2) \end{vmatrix} > 0 \tag{25}$$

$$\begin{vmatrix} \Upsilon_{11} & \Upsilon_{12} & \Upsilon_{13} \\ \Upsilon_{12} & \delta\mathcal{Q}_i(2,2) & \delta\mathcal{Q}_i(2,3) \\ \Upsilon_{13} & \delta\mathcal{Q}_i(2,3) & \delta\mathcal{Q}_i(3,3) \end{vmatrix} < 0 \tag{26}$$

$$\left[\begin{array}{c|c} P_iA_{ii,h} + A_{ii,h}^TP_i + \Psi_{11} & P_iD_i - \mathcal{S}_i \\ \hline * & -\mathcal{R}_i \end{array}\right] < 0 \tag{27}$$

where

$$\begin{aligned} \Upsilon_{11} &= \frac{2P_i(1,1)}{C_{\mathrm{f}i}R_{ij}} + \delta\mathcal{Q}_i(1,1), \\ \Upsilon_{12} &= \frac{P_i(1,2)}{C_{\mathrm{f}i}R_{ij}} + \delta\mathcal{Q}_i(1,2), \\ \Upsilon_{13} &= \frac{P_i(1,3)}{C_{\mathrm{f}i}R_{ij}} + \delta\mathcal{Q}_i(1,3), \\ \Psi_{11} &= P_iB_iK_{i,h} + K_{i,h}^TB_i^TP_i - (1+\delta)\mathcal{Q}_i. \end{aligned}$$

Proof: It is clear that the matrix $\mathbf{\Phi}'_{\mathrm{C}}$ (23b) has only a nonzero entry at position (1,1), while the other entries are zero. By deleting the last two rows and columns, we define $\mathbf{\Xi}_{\mathrm{C}}$ as a description of the remaining item, i.e.,

$$\mathbf{\Xi}_{\mathrm{C}} = \boldsymbol{P}\boldsymbol{A}_{\mathrm{C}} + \boldsymbol{A}_{\mathrm{C}}^T\boldsymbol{P} + \delta\boldsymbol{\mathcal{Q}}. \tag{28}$$

Each block of $\mathbf{\Xi}_{\mathrm{C}}$ is denoted as $\Xi_{\mathrm{C}i}$ in the form of

$$\begin{aligned} \Xi_{\mathrm{C}i} &= P_iA_{ij} + A_{ij}^TP_i + \delta\mathcal{Q}_i \\ &= \begin{bmatrix} \Upsilon_{11} & \Upsilon_{12} & \Upsilon_{13} \\ \Upsilon_{12} & \delta\mathcal{Q}_i(2,2) & \delta\mathcal{Q}_i(2,3) \\ \Upsilon_{13} & \delta\mathcal{Q}_i(2,3) & \delta\mathcal{Q}_i(3,3) \end{bmatrix}. \end{aligned} \tag{29}$$

According to conditions (24)-(26), it can be inferred that the odd-order principal minors of matrix $\Xi_{\mathrm{C}i}$ are less than 0, while the even-order principal minor is greater than 0. Therefore, we can conclude that

$$\Xi_{\mathrm{C}i} < 0. \tag{30}$$

Therefore, one has

$$\mathbf{\Xi}_{\mathrm{C}} < 0 \tag{31}$$

which implies

$$\mathbf{\Phi}'_{\mathrm{C}} = \begin{bmatrix} \boldsymbol{P}\boldsymbol{A}_{\mathrm{C}} + \boldsymbol{A}_{\mathrm{C}}^T\boldsymbol{P} + \delta\boldsymbol{\mathcal{Q}} & \mathbf{0} \\ \mathbf{0} & \mathbf{0} \end{bmatrix} \leq 0. \tag{32}$$

Moreover, by collecting the local dissipativity condition (27), which only captures the local subsystem, one obtains

$$\mathbf{\Phi}'_{\mathrm{D},h} < 0. \tag{33}$$

Thus, according to (32) and (33), we can obtain that the dissipativity of global DCmGs $\mathbf{S}_n$ interconneted with power lines, i.e., $\mathbf{\Phi}_h = \mathbf{\Phi}'_{\mathrm{D},h} + \mathbf{\Phi}'_{\mathrm{C}} < 0$ is guaranteed. Thus, the proof is completed.

Remark 5*:* Note that the adverse effects of power line couplings on the dissipativity of global DCmGs, denoted by $\mathbf{\Phi}'_{\mathrm{C}}$ in (32), can be alleviated by transforming such effects into an LMI condition (28) and subsequently imposing constraints on its sequential principal minors as conditions (24)-(26). Therefore, the dissipativity of global DCmGs can be construed as a simple aggregation of the local dissipativity of each subsystem, irrespective of other subsystems and line couplings. In other words, the dissipativity of global DCmGs can be guaranteed by satisfying the local conditions (24)-(27); each new subsystem will introduce only one additional condition of this kind, rendering the dissipativity conditions scalable with DCmG size and topology.

Remark 6*:* Note that traditional scalable control methods, such as those utilizing the SLF technique, have been widely adopted to mitigate the negative coupling effect of power lines [9], [21]–[25]. However, these methods often encounter limitations, as the block-diagonal fixed structure for Lyapunov matrices can render LMI-based controller designs numerically infeasible or conservative. In contrast, the proposed method avoids such assumptions for Lyapunov matrices, thereby enhancing the solvability and reducing the conservativeness of LMI-based controller designs.

B. Scalable Fuzzy Controller Design

Given that the dissipativity of global DCmGs is ensured by checking the local condition of each subsystem, our emphasis will be concentrated on the design method of scalable fuzzy controller. The corresponding theorem is provided below.

Theorem 2*:* The dissipativity and scalability of closed-loop global DCmGs $\mathbf{S}_n$ interconnected with power lines are guaranteed, if there exists a positive definite matrix $Y_i = [Y_i(p,q)]_{p\in 3,q\in 3}$, symmetric matrices $\mathscr{Q}_i = [\mathscr{Q}_i(p,q)]_{p\in 3,q\in 3}, \mathcal{R}_i$, and suitable matrices $\mathcal{S}_i, X_{i,h}$ for $h = 1,2$ such that the following conditions hold

$$\Pi_{11} < 0 \tag{34}$$

$$\begin{vmatrix} \Pi_{11} & \Pi_{12} \\ \Pi_{12} & \delta\mathscr{Q}_i(2,2) \end{vmatrix} > 0 \tag{35}$$

$$\begin{vmatrix} \Pi_{11} & \Pi_{12} & \Pi_{13} \\ \Pi_{12} & \delta\mathscr{Q}_i(2,2) & \delta\mathscr{Q}_i(2,3) \\ \Pi_{13} & \delta\mathscr{Q}_i(2,3) & \delta\mathscr{Q}_i(3,3) \end{vmatrix} < 0 \tag{36}$$

$$\left[\begin{array}{c|c} A_{ii,h}Y_i + Y_iA_{ii,h}^T + \mathscr{X}_i & D_i - Y_i\mathcal{S}_i \\ \hline * & -\mathcal{R}_i \end{array}\right] < 0 \tag{37}$$

where

$$\begin{aligned}
\Pi_{11} &= \frac{2Y_i(1,1)}{C_{\mathrm{fi}}R_{ij}} + \delta\mathscr{Q}_i(1,1),\\
\Pi_{12} &= \frac{Y_i(1,2)}{C_{\mathrm{fi}}R_{ij}} + \delta\mathscr{Q}_i(1,2),\\
\Pi_{13} &= \frac{Y_i(1,3)}{C_{\mathrm{fi}}R_{ij}} + \delta\mathscr{Q}_i(1,3),\\
\mathscr{X}_i &= B_iX_{i,h} + X_{i,h}^TB_i^T - (1+\delta)\mathscr{Q}_i.
\end{aligned}$$

Then, the scalable fuzzy controller gain $K_{i,h}$ can be parameterized as

$$K_{i,h} = X_{i,h}Y_i^{-1}. \tag{38}$$

Proof: To begin with, we denote

$$Y_i = P_i^{-1}, X_{i,h} = K_{i,h}Y_i, \mathscr{Q}_i = Y_i\mathcal{Q}_iY_i.$$

Then, by performing a congruence transformation to (30) using matrix Y_i, the following matrix inequality holds:

$$\widehat{\Xi}_{\mathrm{C}i} = \left[\begin{array}{ccc} \Pi_{11} & \Pi_{12} & \Pi_{13} \\ \Pi_{12} & \delta\mathscr{Q}_i(2,2) & \delta\mathscr{Q}_i(2,3) \\ \Pi_{13} & \delta\mathscr{Q}_i(2,3) & \delta\mathscr{Q}_i(3,3) \end{array}\right] < 0. \tag{39}$$

According to $\widehat{\Xi}_{\mathrm{C}i} < 0$, it can be inferred that the odd-order principal minors of matrix $\widehat{\Xi}_{\mathrm{C}i}$ are less than 0 while the even-order principal minor is greater than 0. Therefore, conditions (34)-(36) are obtained.

Next, pre- and postmultiply (27) by the diagonal matrix diag $\{Y_i, \mathbf{I}\}$, respectively, and then conditions (37) can be obtained directly. Thus, the proof is completed.

The following Algorithm 1 presents the steps of the scalable fuzzy controller design procedure.

Algorithm 1 Scalable Fuzzy Controller Design Processes

Input: The T-S fuzzy DCmG model $\mathbb{S}_i$ feeding CPL.

Output: Scalable fuzzy controller gain $K_{i,h}$.

1: Give electrical parameters of local subsystem $\mathbb{S}_i$ and the given region ω_i, δ, thereby determining system matrices $A_{ii,h}, B_i, C_i$, and D_i.
2: Define the decision variables in LMI conditions, i.e., $\mathscr{Q}_i, \mathscr{S}_i, \mathscr{R}_i$, and Y_i. Then, obtain matrices Y_i and $X_{i,h}$ by solving LMIs via the YALMIP toolbox in Matlab [43].
3: Finally, if the previous step is feasible, the controller gain $K_{i,h}$ can be computed from $K_{i,h} = Y_{i,h}Y_i^{-1}$.

Remark 7*:* Note that the design method for scalable controllers necessitates only the model of subsystems (DGUs and CPLs); the addition/removal of each subsystem will introduce only one corresponding condition (34)-(37), and thus it exhibits scalability. Moreover, the neighboring subsystems are not obligated to update their local controllers around the plugging-in/-out time. This adherence to privacy requirements aligns well with energy markets, particularly when DGUs have distinct ownership structures [22]. Indeed, the incorporation of DGUs does not necessitate stakeholders to disclose their own DGU models or alter their operational configurations.

C. PnP Operations of Subsystem

In this section, we describe the operations necessary for plugging-in/-out subsystems (DGUs and CPLs) while maintaining the dissipativity of DCmGs. An illustrative example is depicted in Fig. 3.

Plugging-in operation: Given an interconnected dissipative DCmG $\mathbf{S}_n$ equipped with scalable fuzzy controller $\boldsymbol{K}_h$, which collects the local controllers $K_{i,h}$ produced by Algorithm 1. A new subsystem $\mathbb{S}_{n+1}$ is allowed to plug in $\mathbf{S}_n$, resulting in a new DCmG denoted as $\mathbf{S}_{n+1} = \mathbf{S}_n|\mathbb{S}_{n+1}^+$, which maintains dissipativity if the local controller $K_{n+1,h}$ necessitates the execution of Algorithm 1.

Plugging-out operation: The unplugging of a subsystem is even simpler since it has no impact on the controllers of the remaining units. Given an interconnected DCmG $\mathbf{S}_n$ with scalable fuzzy controller $\boldsymbol{K}_h$, an arbitrary subsystem can be plugged out directly, and the remaining DCmG, represented by $\mathbf{S}_{n-1} = \mathbf{S}_n|\mathbb{S}_{n-1}^-$, also maintains dissipativity because the equipped local controller $K_{n-1,h}$ requires only the model of the individual subsystem.

TABLE II
SCALABLE FUZZY CONTROLLER GAIN $K_{i,h}$ OF DCMG SUBSYSTEM

Subsystem $\mathbb{S}_i$	Controller gain $K_{i,h}$ of $\mathbb{C}_i$			
$\mathbb{S}_1$	$K_{1,1} =$	-5.164	-0.072	50.829
	$K_{1,2} =$	-4.983	-0.065	50.817
$\mathbb{S}_2$	$K_{2,1} =$	-7.006	-0.048	45.261
	$K_{2,2} =$	-6.973	-0.057	44.915
$\mathbb{S}_3$	$K_{3,1} =$	-6.019	-0.083	36.217
	$K_{3,2} =$	-6.301	-0.089	35.584
$\mathbb{S}_4$	$K_{4,1} =$	-5.871	-0.075	91.495
	$K_{4,2} =$	-6.028	-0.091	90.283
$\mathbb{S}_5$	$K_{5,1} =$	-6.714	-0.024	60.738
	$K_{5,2} =$	-6.899	-0.016	61.907
$\mathbb{S}_6$	$K_{6,1} =$	-9.004	-0.027	52.914
	$K_{6,2} =$	-8.948	-0.031	55.102

V. SIMULATION RESULTS

In this section, we present the validation of the proposed scalable fuzzy control scheme through realistic computer simulations using the Specialized Matlab/SimPowerSystems toolbox. As depicted in Fig. 3, the considered DCmGs topology comprises six DGUs feeding on CPLs with $\mathcal{P}_1 = 380$W, $\mathcal{P}_2 = 350$W, $\mathcal{P}_3 = 400$W, $\mathcal{P}_4 = 360$W, $\mathcal{P}_5 = 370$W, and $\mathcal{P}_6 = 390$W; each of them is equipped with the proposed controllers $\mathbb{C}_i, i = 1, 2, ..., 6$. The electrical parameters

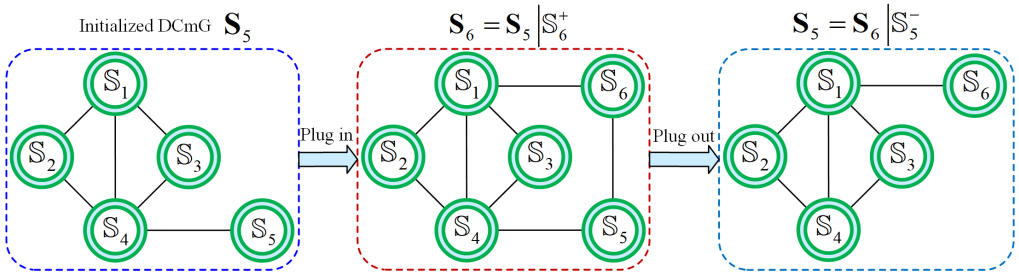

Fig. 3. Illustration for plugging-in/-out operations.

of subsystems are taken from [21]. The voltage references $U_1^* = 47$V, $U_2^* = 48$V, $U_3^* = 45$V, $U_4^* = 50$V, $U_5^* = 46$V, and $U_6^* = 49$V. The equilibrium point voltage is chosen as $U_{0i} = U_i^*$. Based on these provided parameters, the controller gains $K_{i,h}$ for $h = 1, 2$ are computed using Algorithm 1, and the results are presented in Table II.

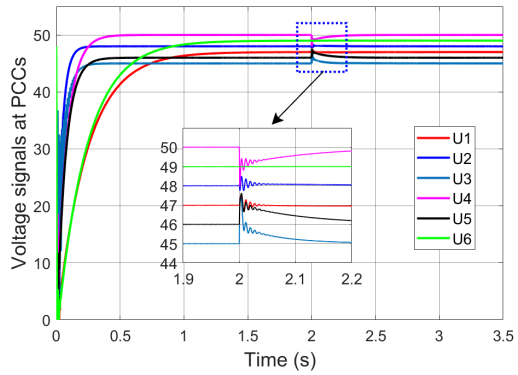

(a) Voltage tracking

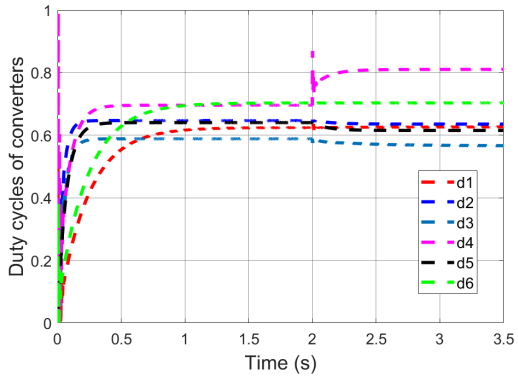

(b) Control input

Fig. 4. Initialization of DCmGs with local controllers at the beginning, and then interconnection of DGUs 1–5 via power lines at $t = 2$s.

Initialization of the DCmG: At the initial time, i.e., $t = 0$s, DGUs 1–6 are initialized with all power lines disconnected, resulting in no power transfer between them. At this stage, the proposed scalable fuzzy controllers $K_{i,h}, i = 1, 2, ..., 6, h = 1, 2$ (shown in Table II) regulate PCCs voltages to their reference values U_i^*, during which CPLs are supplied by all DGUs. At $t = 2$s, DGUs 1–5 are interconnected to form a DCmG system $\mathbf{S}_5$, while $\mathbb{S}_6$ is disconnected from the rest of the DCmG.

The simulation results for the initialization process are shown in Fig. 4, including (a): voltage signals at PCCs and (b): duty cycles of converters. Note that since the control signal is $u_i = d_i U_{si}$, only the duty cycle d_i is shown in Fig. 4(b). From Fig. 4(a), it is evident that minor voltage deviations from their reference values are produced but quickly disappear.

A. Case 1: Scalable Performance for PnP operations

In this case, the scalable performance of the proposed control scheme is analyzed by plugging in and unplugging subsystems (DGUs and loads), respectively.

Scalability for plugging-in operation: We plug in $\mathbb{S}_6$ at $t = 4$s. As depicted in Fig. 5(a), the PCCs voltage signals produce small deviations from their set-point references around the operation time, which recover after a very short time. The control signals are shown in Fig. 5(b). The simulation results reveal the scalable performance of the proposed voltage controllers under plugging-in operation.

Scalability for plugging-out operation: Then, at $t = 6$s, $\mathbb{S}_5$ is unplugged. The voltage and control signals are depicted in Fig. 6. It is clear that voltage signals do not significantly deviate from their voltage references, and the deviations disappear quickly. Therefore, the scalable performance of unplugging subsystems is ensured by the proposed control scheme.

B. Case 2: Robust Performance for Varying Power of CPLs

The case study assesses the robust performance of the proposed control scheme in response to varying power demands of CPLs. We assume that the power $\mathcal{P}_i$ of CPLs changes at $t = 8$s. Specifically, $\mathcal{P}_1$ increases from 380W to 456W, $\mathcal{P}_2$ increases from 350W to 420W, $\mathcal{P}_3$ decreases from 400W to 320W, $\mathcal{P}_4$ decreases from 360W to 324W, $\mathcal{P}_5$ increases from 370W to 407W, and $\mathcal{P}_6$ decreases from 390W to 351W. The voltage signals at PCCs are depicted in Fig. 7(a), and the control signals are shown in Fig. 7(b). The results illustrate that the fluctuating power demands of CPLs do not adversely affect the voltage stability. Hence, the proposed control method exhibits robustness against varying power demands of CPLs.

C. Case 3: Robust Performance for Varying Voltage References

The case evaluates the robust performance against varying voltage references, with U_1^* increased to 50V and U_2^* decreased to 45V at $t = 10$s. The dynamic responses of voltage tracking are depicted in Fig. 8(a), while Fig. 8(b) illustrates the corresponding control signals. The results demonstrate that the proposed control method effectively maintains the voltage

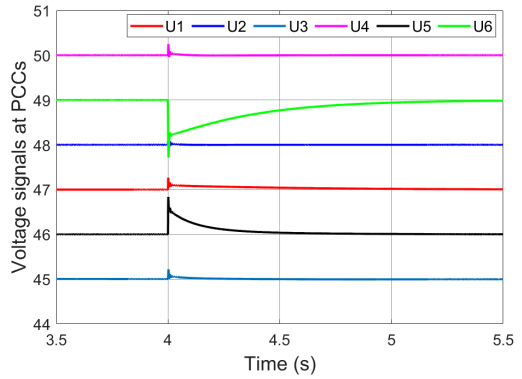

(a) Voltage tracking

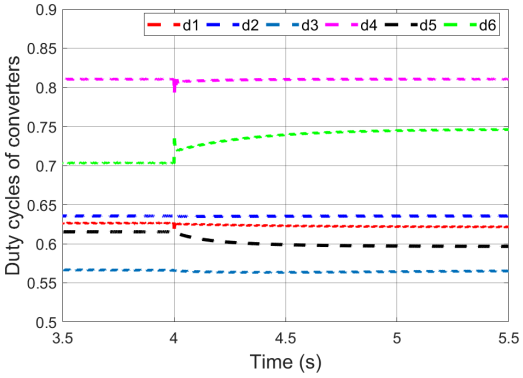

(b) Control input

Fig. 5. Scalable performance for plugging-in $\mathbb{S}_6$ at $t = 4$s.

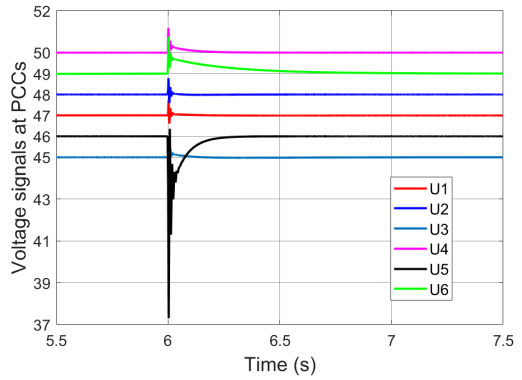

(a) Voltage tracking

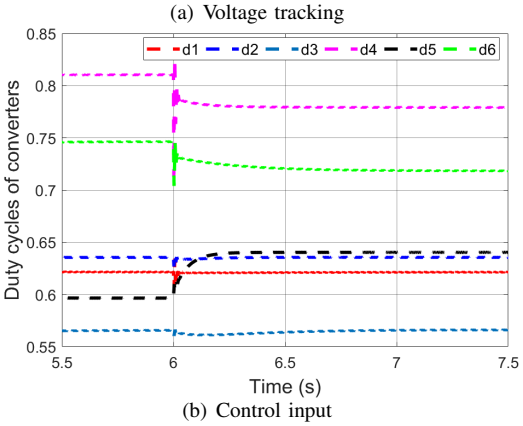

(b) Control input

Fig. 6. Scalable performance for unplugging $\mathbb{S}_5$ at $t = 6$s.

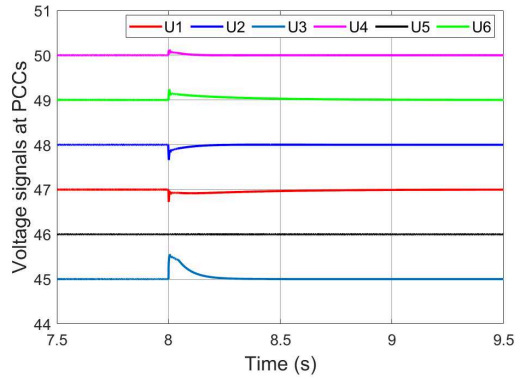

(a) Voltage tracking

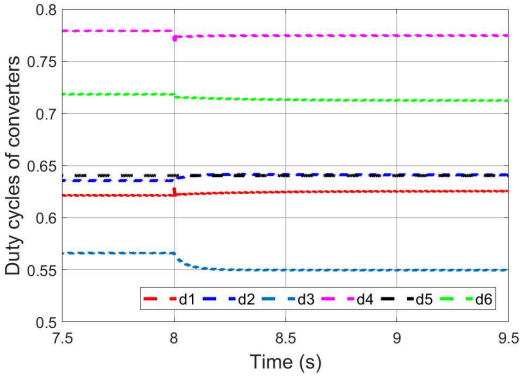

(b) Control input

Fig. 7. Robust performance for varying power demands of CPLs at $t = 8$s.

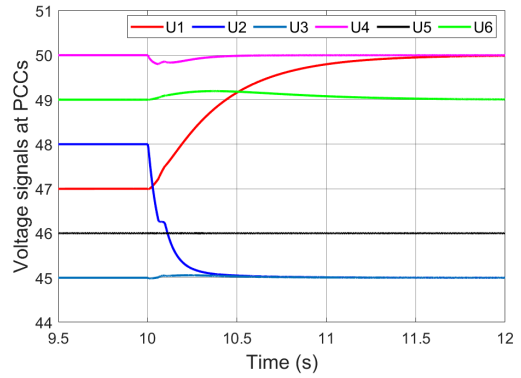

(a) Voltage tracking

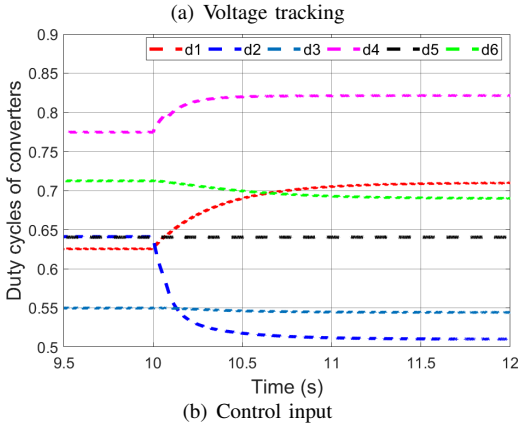

(b) Control input

Fig. 8. Robust performance for varying voltage references at $t = 10$s.

signals at PCCs with negligible steady-state error and minimal transient time. In other words, the proposed control method manifests robustness to varying voltage references.

VI. Conclusion

This paper has proposed a scalable fuzzy voltage control for DCmGs under PnP operations with CPLs. Firstly, the T-S fuzzy system was modeled to address the nonlinearity of CPLs. Secondly, a scalable fuzzy control scheme was proposed, supported by a novel argument based on LMI constraints on sequential principal minors representing line couplings. This scalable control scheme enables DGUs to be seamlessly plugged in or out without requiring adjustments to their local controllers. Finally, the effectiveness of the proposed control method was verified through simulation studies in the MATLAB/SimPowerSystems toolbox. Future work includes extending this scalable approach to address advanced objectives in cyber-physical DCmGs, such as current and power sharing.

References

[1] F. Yang, X. Xie, and C. Peng, "Co-design of new fuzzy switching-type state-FDI estimation and attack compensation for DC microgrids under hybrid attacks," *IEEE Trans. Fuzzy Syst.*, vol. 32, no. 4, pp. 1743–1755, Apr. 2024.

[2] J. -N. Li, H. Feng, Y. Wang, and G. -Y. Liu, "A novel failure-distribution-dependent non-fragile H_∞ fault-tolerant load frequency control for faulty multi-area power systems," *IEEE Trans. Power Syst.*, vol. 39, no. 2, pp. 2936–2946, Mar. 2024.

[3] M. Liu, F. Teng, Z. Zhang, P. Ge, M. Sun, R. Deng, P. Cheng, and J. Chen "Enhancing cyber-resiliency of DER-based smart grid: A survey," *IEEE Trans. Smart Grid*, early access, Mar. 05, 2024, doi: 10.1109/TSG.2024.3373008.

[4] D. Du, M. Zhu, X. Li, M. Fei, S. Bu, L. Wu, and K. Li, "A review on cybersecurity analysis, attack detection, and attack defense methods in cyber-physical power systems," *J. Mod. Power Syst. Clean Energy*, vol. 11, no. 3, pp. 727–743, May 2023.

[5] B. Cao, W. Dong, Z. Lv, Y. Gu, S. Singh, and P. Kumar, "Hybrid microgrid many-objective sizing optimization with fuzzy decision," *IEEE Trans. Fuzzy Syst.*, vol. 28, no. 11, pp. 2702–2710, Nov. 2020.

[6] P. Mani and Y. H. Joo, "Fuzzy event-triggered control for back-to-back converter involved PMSG-based wind turbine systems," *IEEE Trans. Fuzzy Syst.*, vol. 30, no. 5, pp. 1409–1420, May 2022.

[7] A. Wang, M. Fei, and Y. Song, "A novel scalable and reliable control for DC microgrids with varying number of agents," *IEEE Trans. Cybern.*, early access, Feb. 26, 2024, doi: 10.1109/TCYB.2024.3363779.

[8] M. Liu, C. Zhao, J. Xia, R. Deng, P. Cheng, and J. Chen, "PDDL: Proactive distributed detection and localization against stealthy deception attacks in DC microgrids," *IEEE Trans. Smart Grid*, vol. 14, no. 1, pp. 714–731, Jan. 2023.

[9] S. Riverso, F. Sarzo, and G. Ferrari-Trecate, "Plug-and-play voltage and frequency control of islanded microgrids with meshed topology," *IEEE Trans. Smart Grid*, vol. 6, no. 3, pp. 1176–1184, May 2015.

[10] S. Hu, P. Yuan, D. Yue, C. Dou, Z. Cheng, and Y. Zhang, "Attack-resilient event-triggered controller design of DC microgrids under DoS attacks," *IEEE Trans. Circuits Syst. I-Regul. Pap.*, vol. 67, no. 2, pp. 699–710, Feb. 2020.

[11] J. Su, K. Li, and C. Xing, "Plug-and-play of grid-forming units in DC microgrids assisted with power buffers," *IEEE Trans. Smart Grid*, vol. 15, no. 2, pp. 1213–1226, Mar. 2024.

[12] C. Deng, F. Guo, C. Wen, D. Yue, and Y. Wang, "Distributed resilient secondary control for DC microgrids against heterogeneous communication delays and DoS attacks," *IEEE Trans. Ind. Electron.*, vol. 69, no. 11, pp. 11560–11568, Nov. 2022.

[13] M. Liu, C. Zhao, Z. Zhang, R. Deng, P. Cheng, and J. Chen, "Converter-based moving target defense against deception attacks in DC microgrids," *IEEE Trans. Smart Grid*, vol. 13, no. 5, pp. 3984–3996, Sep. 2022.

[14] T. Dragičević, X. Lu, J. C. Vasquez, and J. M. Guerrero, "DC microgrids–Part II: A review of power architectures, applications, and standardization issues," *IEEE Trans. Power Electron.*, vol. 31, no. 5, pp. 3528–3549, May 2016.

[15] R. Griñó, R. Ortega, E. Fridman, J. Zhang, and F. Mazenc, "A behavioural dynamic model for constant power loads in single-phase AC systems," *Automatica*, vol. 131, Sep. 2021, Art. no. 109744.

[16] D. Zonetti, R. Ortega, and J. Schiffer, "A tool for stability and power-sharing analysis of a generalized class of droop controllers for high-voltage direct-current transmission systems," *IEEE Trans. Control Netw. Syst.*, vol. 5, no. 3, pp. 1110–1119, Sep. 2018.

[17] Q. Xu, C. Zhang, C. Wen, and P. Wang, "A novel composite nonlinear controller for stabilization of constant power load in DC microgrid," *IEEE Trans. Smart Grid*, vol. 10, no. 1, pp. 752–761, Jan. 2019.

[18] J. Liu, W. Zhang, and G. Rizzoni, "Robust stability analysis of DC microgrids with constant power loads," *IEEE Trans. Power Syst.*, vol. 33, no. 1, pp. 851–860, Jan. 2018.

[19] M. Gheisarnejad, A. Akhbari, M. Rahimi, B. Andresen, and M. -H. Khooban, "Reducing impact of constant power loads on DC energy systems by artificial intelligence," *IEEE Trans. Circuits Syst. II–Express Briefs*, vol. 69, no. 12, pp. 4974–4978, Dec. 2022.

[20] S. Dasgupta, S. N. Mohan, S. K. Sahoo, and S. K. Panda, "A plug and play operational approach for implementation of an autonomous-microgrid system," *IEEE Trans. Ind. Inform.*, vol. 8, no. 3, pp. 615–629, Aug. 2012.

[21] M. Tucci, S. Riverso, J. C. Vasquez, J. M. Guerrero, and G. Ferrari-Trecate, "A decentralized scalable approach to voltage control of DC islanded microgrids," *IEEE Trans. Control Syst. Technol.*, vol. 24, no. 6, pp. 1965–1979, Nov. 2016.

[22] M. Tucci, S. Riverso, and G. Ferrari-Trecate, "Line-independent plug-and-play controllers for voltage stabilization in DC microgrids," *IEEE Trans. Control Syst. Technol.*, vol. 26, no. 3, pp. 1115–1123, May 2018.

[23] A. Wang, M. Fei, D. Du, and Y. Song, "A novel scalable fault-tolerant control design for DC microgrids with nonuniform faults," *IEEE/CAA J. Autom. Sinica*, early access, Nov. 2, 2023, doi: 10.1109/JAS.2023.123918.

[24] P. Nahata, R. Soloperto, M. Tucci, A. Martinelli, and G. Ferrari-Trecate, "A passivity-based approach to voltage stabilization in DC microgrids with ZIP loads," *Automatica*, vol. 113, Mar. 2020, Art. no. 108770.

[25] M. Tucci and G. Ferrari-Trecate, "A scalable, line-independent control design algorithm for voltage and frequency stabilization in AC islanded microgrids," *Automatica*, vol. 111, Jan. 2020, Art. no. 108577.

[26] T. Dragičević, X. Lu, J. C. Vasquez, and J. M. Guerrero, "DC microgrids–Part I: A review of control strategies and stabilization techniques," *IEEE Trans. Power Electron.*, vol. 31, no. 7, pp. 4876–4891, Jul. 2016.

[27] P. Nahata, M. S. Turan, and G. Ferrari-Trecate, "Consensus-based current sharing and voltage balancing in DC microgrids with exponential loads," *IEEE Trans. Control Syst. Technol.*, vol. 30, no. 4, pp. 1668–1680, Jul. 2022.

[28] F. Dörfler and F. Bullo, "Kron reduction of graphs with applications to electrical networks," *IEEE Trans. Circuits Syst. I–Regul. Pap.*, vol. 60, no. 1, pp. 150–163, Jan. 2013.

[29] V. Venkatasubramanian, H. Schattler, and J. Zaborszky, "Fast time-varying phasor analysis in the balanced three-phase large electric power system," *IEEE Trans. Autom. Control*, vol. 40, no. 11, pp. 1975–1982, Nov. 1995.

[30] S. Skogestad and I. Postlethwaite, *Multivariable Feedback Control: Analysis and Design*. New York, NY, USA: Wiley, 1996.

[31] L. Herrera, W. Zhang, and J. Wang, "Stability analysis and controller design of DC microgrids with constant power loads," *IEEE Trans. Smart Grid*, vol. 8, no. 2, pp. 881–888, Mar. 2017.

[32] M. M. Mardani, N. Vafamand, M. H. Khooban, T. Dragičević, and F. Blaabjerg, "Design of quadratic D-stable fuzzy controller for DC microgrids with multiple CPLs," *IEEE Trans. Ind. Electron.*, vol. 66, no. 6, pp. 4805–4812, Jun. 2019.

[33] D. K. Fulwani and S. Singh, *Mitigation of Negative Impedance Instabilities in DC Distribution Systems–A Sliding Mode Control Approach*. Berlin, Germany: Springer, 2016.

[34] D. Bosich, G. Giadrossi, and G. Sulligoi, "Voltage control solutions to face the CPL instability in MVDC shipboard power systems," *in Proc. AEIT Annu. Conf. Res. Ind. Need More Effect. Technol. Transfer (AEIT)*, Trieste, Italy, Sep. 2014, pp. 1–6.

[35] S. J. Kim and I. -J. Ha, "A state-space approach to analysis of almost periodic nonlinear systems with sector nonlinearities," *IEEE Trans. Autom. Control*, vol. 44, no. 1, pp. 66–70, Jan. 1999.

[36] H. K. Lam, C. Liu, L. Wu, and X. Zhao, "Polynomial fuzzy-model-based control systems: Stability analysis via approximated membership functions considering sector nonlinearity of control input," *IEEE Trans. Fuzzy Syst.*, vol. 23, no. 6, pp. 2202–2214, Dec. 2015.

[37] J. Dong and G. Yang, "Control synthesis of TS fuzzy systems based on a new control scheme," *IEEE Trans. Fuzzy Syst.*, vol. 19, no. 2, pp. 323–338, Apr. 2011.

[38] K. Tanaka and H. O. Wang, *Fuzzy Control Systems Design and Analysis*. New York, NY, USA: Wiley, 2001.
[39] Z. Xiang, P. Li, M. Chadli, and W. Zou, "Fuzzy optimal control for a class of discrete-time switched nonlinear systems," *IEEE Trans. Fuzzy Syst.*, vol. 32, no. 4, pp. 2297–2306, Apr. 2024.
[40] D. Cui, M. Chadli, and Z. Xiang, "Fuzzy fault-tolerant predefined-time control for switched systems: A singularity-free method," *IEEE Trans. Fuzzy Syst.*, vol. 32, no. 3, pp. 1223–1232, Mar. 2024.
[41] W. J. Rugh, *Linear System Theory*, Prentice-Hall, Inc,1996.
[42] E. Agarwal, S. Sivaranjani, V. Gupta, and P. J. Antsaklis, "Distributed synthesis of local controllers for networked systems with arbitrary interconnection topologies," *IEEE Trans. Autom. Control*, vol. 66, no. 2, pp. 683–698, Feb. 2021.
[43] J. Löfberg, "YALMIP: A toolbox for modeling and optimization in matlab," *Proc. IEEE Int. Symp. Comput. Aided Control Syst. Des.*, pp. 284–289, 2004.